Analytical and Theoretical Development of Load-Moment Interaction Diagrams of Rectangular CFRP-RC Columns

Mohannad H. Al-Sherrawi
Department of Civil Engineering, University of Baghdad, Baghdad, Iraq
dr.mohannad.al-sherrawi@coeng.uobaghdad.edu.iq

Hamza M. Salman
Department of Civil Engineering, University of Baghdad, Baghdad, Iraq
hamza.m@coeng.uobaghdad.edu.iq (corresponding author)

Shatha D. Mohammed
Department of Civil Engineering, University of Baghdad, Baghdad, Iraq
shatha.dh@coeng.uobaghdad.edu.iq

Received: 11 May 2025 | Revised: 26 May 2025 | Accepted: 6 June 2025

 DOI: https://doi.org/10.48084/etasr.12059

ABSTRACT

Carbon Fiber-Reinforced Polymer (CFRP) bars have several advantages over traditional steel reinforcement, including low density, erosion resistance, and higher tensile strength. The ACI 440.11-22 code permits CFRP as reinforcement; however, there are limited experimental studies on its application in Reinforced Concrete (RC) columns under combined loads. This study utilized theoretical analysis and Finite Element Analysis (FEA) to investigate 25 square slender concrete columns (kL/r = 17) affected by concentric and eccentric loads, examining variables, like CFRP bar contribution, eccentricity-to-depth ratio, and reinforcement arrangement. The results demonstrated CFRP's effectiveness in these columns, with failure modes varying from brittle compression-controlled under low eccentricities to tension-controlled under high eccentricities. The FEA results indicated that the CFRP columns exhibited higher second-order moments than the steel columns due to CFRP's lower elastic modulus, these results were compatible with the experimental results. Moreover; the (P-M) interaction diagram of CFRP reinforced column does not experience a balanced point. It was also observed that increasing the reinforcement ratio enhances the axial capacity by 33% and the bending resistance by 141% while reducing the ties' spacing from 140 mm to 40 mm has no significant influence on both the axial capacity and bending resistance. The study also expanded to verify theoretical models against experimental data, confirming their accuracy. These findings contribute to establishing reliable design guidelines for CFRP-RC columns influenced by axial loads and bending moments.

Keywords-CFRP reinforcement; concrete columns; eccentricity level; P-M interaction diagram; second-order moment

I. INTRODUCTION

Fiber-Reinforced Polymer (FRP) bars are becoming popular as an alternative to steel bars in RC structures. They offer advantages, such as corrosion resistance, a high strength-to-weight ratio, and long-term durability, making them a preferred choice in construction [1]. FRP bars' compressive strength is generally lower than their ultimate tensile strength. This difference is due to factors, like the fiber content, testing procedure, and resin quality. There are standard test methods available to measure the tensile properties of FRP bars [2-3]. Testing the latter's compression is difficult due to their unique properties, while no standard procedure exists for this type of testing. Despite this, various compression test methods have been introduced, while it has been indicated that the compressive strength of FRP bars is usually between 10% and 65% of their ultimate tensile strength [4-7].

Columns are essential in RC structures; the failure of just one can cause a building to collapse. Thus, analyzing and designing RC columns is crucial. Research has focused on the performance of Glass Fiber-Reinforced Polymer (GFRP) and CFRP in short concrete columns [8-11]. Experimental studies indicate that the longitudinal reinforcement from FRP bars enhances the load-carrying capability of concentrically loaded columns. Specifically, GFRP bars contribute between 3% and

10%, while CFRP bars contribute between 6% and 19%. Although the influence of FRP bars can be ignored in eccentrically loaded columns due to a potential buckling failure before bar rupture, this could lead to an underestimation of the column's capacity [12-13].

The behavior of concrete columns reinforced with FRP bars and ties under axial and flexural loads has not been thoroughly investigated, with FRP bars not being a part of construction design strategies and standards. Authors in [14] studied BFRP-reinforced inorganic polymer short concrete columns (120 mm × 120 mm × 900 mm) under eccentric loads and found that their performance is comparable to that of steel-RC columns, but with a 30% lower load-carrying capacity. Authors in [15] investigated the axial and flexural performance of square concrete members reinforced with GFRP bars and encased with pultruded GFRP structural sections under a variety of loading conditions. An analytical model was designed to accurately predict the axial load-bending moment interaction diagrams of the tested specimens. The results demonstrated that these analytical models yield highly reliable estimations of the ultimate load and bending moment limits for the GFRP-reinforced and GFRP-encased concrete columns, showcasing their effectiveness in structural applications. In [16], fifteen CFRP-reinforced rectangular concrete columns and three steel-reinforced columns were tested under various eccentric loads. The key parameters included the use of CFRP bars instead of steel, load eccentricity, percentage of the longitudinal reinforcement, and tie spacing. The results showed that the CFRP columns behaved similarly to the steel-reinforced columns, with minor axial and flexural capacity differences. Increasing the CFRP longitudinal reinforcement ratios improved the ultimate strength for different eccentricities. Authors in [17] experimentally and analytically examined the behavior of short and slender concrete columns reinforced with Basalt Fiber-Reinforced Polymer (BFRP) bars under axial and flexural loads. A total of twelve concrete columns were constructed and tested under four different load eccentricity-to-depth (*e/d*) ratios to develop axial load–moment interaction diagrams. The experimental results demonstrated that the BFRP bars are effective in reinforcing both short and slender concrete columns when subjected to concentric and eccentric loading conditions. Authors in [10] conducted both experimental and analytical investigations on ten full-scale circular concrete columns reinforced with CFRP bars and spirals. These columns were tested under combined axial compression and bending moments, with the key variables including varying eccentricity-to-diameter (*e/d*) ratios and two types of reinforcement—CFRP and conventional steel. The study revealed that columns reinforced with CFRP and steel exhibited a comparable behavior in terms of their peak load capacities. However, the CFRP-reinforced columns showed reduced load-bearing capacity and flexural strength compared to their steel-reinforced counterparts across all eccentricity levels—low, moderate, and high. Notably, the failure in CFRP-RC columns did not result from tensile rupture of the reinforcement. The findings suggest that CFRP can be effectively used in eccentrically loaded columns, provided that the compressive stress in the reinforcement is limited to less than 40% of its ultimate tensile strength. CFRP bars contribute to both the tensile and compressive resistance, and neglecting their compressive role can lead to an underestimation of the total axial load capacity.

This study builds on previous experimental and theoretical research using Finite Element (FE) and theoretical models to predict the load-interaction diagrams for square concrete specimens reinforced with CFRP. It aims to validate the experimental results from [16]. The key parameters examined include the load eccentricity, internal reinforcement type, and the performance of the CFRP-reinforced columns under compressive and flexural loading, eccentricity levels, CFRP reinforcement ratios, and transverse reinforcement arrangements, as well as the contribution of CFRP bars to axial and flexural resistance.

II. FINITE ELEMENT MODEL

The Abaqus/CAE 2017 software was used in the FE model generation. The CFRP bars were represented using the truss elements T3D2, which are two-node elements with three translational degrees of freedom at each node. The geometric effects of second-order analysis, the concrete non-linear characteristics, and the attendance of interfacing between the CFRP bars and concrete were considered. The Concrete Damage Plasticity (CDP) model was used to define the concrete material. The CDP model is a modification of the strength hypothesis presented by Drucker–Preger. This model is suitable for modeling concrete and any quasi-brittle materials [18], modeling different types of structures like solids, beams, trusses, shells, and modeling plain and reinforced concrete. Two failure mechanisms were assumed in the CDP model: (1) concrete cracking and (2) concrete crushing. To define the CDP model, the modulus of elasticity for the concrete, Poisson's ratio, the damage plasticity parameters, and the behavior of concrete in both compression and tension must be provided. Five damage parameters were used in the CDP model, as shown in Table I. All the parameters are of standard values except the dilation angle (ψ), which ranges between 31-51 degrees.

TABLE I. CDP PARAMETERS

Parameter	ψ	ε_{fp}	f_{b0}/f_{c0}	K_c	μ
Value	36	0.1	1.16	0.667	0

In Table I, ψ is the dilation angle in degrees, ε_{fp} is the flow potential eccentricity, f_{b0}/f_{c0} is the ratio of the initial biaxial compressive yield stress to the initial uniaxial compressive yield stress, K_c is the ratio of the second stress invariant on the tensile meridian to that on the compressive meridian, and μ is the concrete viscosity. The compressive stress developed in the case of unconfined concrete was presented, in terms of the strains, by the stress-strain model [19]:

$$f_c = \left[\frac{(\alpha+1)\left(\frac{\varepsilon_c}{\varepsilon_{co}}\right)}{\left(\frac{\varepsilon_c}{\varepsilon_{co}}\right)^{\alpha+1}+\alpha}\right] f_{co} \quad (1)$$

where f_c is the compressive stress related to the compressive strain ε_c, f_{co} is the unconfined concrete strength, equal to 85% of the compressive cylinder strength. ε_{co} represents the strain for f_{co} in (6), and α determines the slopes of the ascending and

descending branches of the stress-strain relationship. For the ascending part, (2) was adopted, while (3) was considered for the descending portion:

$$\alpha = 0.2e^{(0.73\xi)} \; for \; \varepsilon_c \leq \varepsilon_{co} \quad (2)$$

$$\alpha = 0.41e^{(0.77\xi)} \; for \; \varepsilon_c > \varepsilon_{co} \quad (3)$$

$$\xi = 0.95(0.1f_{co})^{0.67} \quad (4)$$

The elastic modulus (E_c) was calculated using the ACI 318-19 suggested equation:

$$E_c = 4700\sqrt{f_{co}} \quad (5)$$

$$\varepsilon_{co} = 0.0016e^{240\left(\frac{f_{co}}{E_c}\right)} \quad (6)$$

The concrete tension behavior in the damage model is characterized by two distinct phases: the linear part, which is the elastic portion starting at a stress equal to zero and ending with a stress equal to the concrete tensile strength, and the nonlinear post-peak portion, which is called the tension stiffening. The model presented in [20] was used to plot the stress-strain curve:

$$f_t = E_c\varepsilon_t \; for \; \varepsilon_t \leq \varepsilon_{cr} \quad (7)$$

$$f_t = f_{ct}\left(\frac{\varepsilon_{cr}}{\varepsilon_t}\right)^{0.4} for \; \varepsilon_t > \varepsilon_{cr} \quad (8)$$

where ε_{cr} is the cracking strain that is determined by:

$$\varepsilon_{cr} = \frac{f_{ct}}{E_c} \quad (9)$$

where f_{ct} is the concrete tensile strength and it can be obtained from [21]:

$$f_{ct} = 0.33\sqrt{f_{co}} \quad (10)$$

The CFRP bars exhibit various failure modes under compression, such as transverse tensile failure, fiber micro buckling, and shear failure [22]. It is crucial to determine the compression behavior of FRP bars for the design of CFRP-RC columns. FRP bars generally have lower compressive strength compared to their tensile strength. In tension, CFRP reinforcing bars show a linear, brittle behavior until failure. It has been indicated that the tensile testing of the stress-strain response of the CFRP bars follows an idealized linear elastic behavior. The "embedded region" module of Abaqus was used to simulate the interaction between the concrete and CFRP reinforcing bars. A full composite interaction was presumed between the two different materials.

III. THEORETICAL ANALYSIS

This section presents the calculations for the theoretical axial capacity and bending moment of CFRP-reinforced columns at different levels of eccentricity. The theoretical analysis involves developing the axial load-bending moment (P-M) interaction diagrams. Seven mathematical methods and codes from previous research were modified and used in this study. For each method, P-M was drawn based on six points. The first point represents the axial load resistance of the specimens under concentric loading (zero eccentricity). The next four points represent the axial load and bending moment resistance for specimens loaded with eccentricity levels (*e/h*) 25%, 50%, 75%, and 100%, respectively. The last point represents the bending resistance only, i.e., the specimens sustain pure bending moment. For any point of loading, the general predicted equation for the different used methods is explained in Table II. This analysis uses the strain compatibility and internal force equilibrium for the column's cross-section [23], as depicted in Figure 2. A linear stress-strain profile for CFRP bars was utilized to calculate the forces from compression and tension. The compression values were considered positive, while the tensile values were negative. Assumptions, like those for the steel-reinforced cross-sections, were used to create P-M diagrams. These assumptions were:

- Linear distribution of the strain along the column's depth.
- The strain in the CFRP bars and concrete is directly proportional to the neutral axis location.
- Strain compatibility and ideal bond between the different materials is assumed.
- The ultimate applicable strain at the concrete compression fibers is 0.003 and the tensile strength is ignored, as per ACI 440.11-22 [1]
- The rectangular stress block describes the distribution of concrete compressive stress.
- The CFRP reinforcing bars are made of a linear brittle material with orthotropic characteristics.
- The confinement effects of CFRP transverse reinforcement are ignored.
- The column specimens were treated as short elements, and the slenderness effects were neglected in developing the axial load–moment (P–M) interaction diagrams.

In Table II, f_c' is the concrete compressive strength, c is the position on the neutral axis, b is the column width, A_f is the total area of the longitudinal CFRP reinforcement, F_{ft} is the stress of the CFRP bars in the tension zone, F_{fc} is the stress of the CFRP bars in the compression zone, h is the depth of the column, d and d_1 are the effective depth of the CFRP bars in the tension and compression zone. β_1 can be calculated with:

$$\beta_1 = 0.85 - 0.0015f_c' \geq 0.67 \quad (11)$$

$$\varepsilon_{ft} = \varepsilon_c\left(\frac{d}{c} - 1\right) \quad (12)$$

$$\varepsilon_{fc} = \varepsilon_c\left(1 - \frac{d_1}{c}\right) \quad (13)$$

where ε_{ft} and ε_{fc} in (12) and (13) are the strains of the CFRP bars in the tension and compression zones, respectively. Also, E_f is the modulus of elasticity of the CFRP bars, ε_c is the concrete crushing strain, which is assumed to be 0.003. ACI 440.11-22 ignores the compressive contribution of CFRP bars in the axial load-carrying capacity of the columns. Authors in [13] noted that only 35% of the CFRP bar's ultimate tensile stress can be used in the contribution of CFRP bars in the compression zone. In [5, 9], it was noted that the strain in the CFRP bars lying in the compression zone must not exceed the unconfined concrete strain, which is assumed to be 0.002.

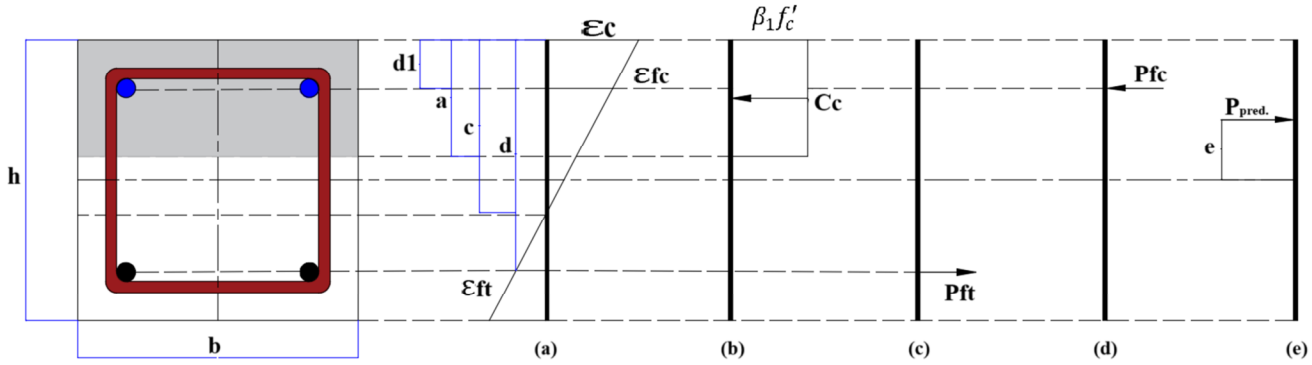

Fig. 1. Rectangular stress block and force distribution of CFRP reinforcement: (a) strain distribution, (b) concrete stress distribution, (c) tensile force, (d) compression force, (e) resultant force.

TABLE II. MODIFICATION OF THEORETICAL MODELS FOR AXIAL LOAD AND BENDING MOMENT CAPACITY FROM LITERATURE

Code	Ref.	*P*			*M*
		P_C	P_{ft}	P_{fc}	
Pre.1	[1]	$0.85 f_c' \, b \, c$	$\frac{A_f}{2} \varepsilon_{ft} E_f \leq \frac{A_f}{2} \varepsilon_{fy} E_f$	-	$\left[P_c\left(\frac{h-0.85c}{2}\right)\right] \mp \left[P_{ft}\left(d-\frac{h}{2}\right)\right] \mp \left[P_{fc}\left(\frac{h}{2}-d_1\right)\right]$
Pre.2	[13]			$f_{fc} \frac{A_f}{2} \leq 0.35 f_{fy} \frac{A_f}{2}$	
Pre.3	[9]			$\varepsilon_{fc} E_f \frac{A_f}{2} \leq 0.002 E_f \frac{A_f}{2}$	
Pre.4	[24]			$\varepsilon_{fc} E_f \frac{A_f}{2} \leq \varepsilon_{co} E_f \frac{A_f}{2}$	
Pre.5	[25]			$\varepsilon_{fc} E_f \frac{A_f}{2} \leq 0.003 E_f \frac{A_f}{2}$	
Pre.6	[5]	$0.9 f_c' \, b \, c$		$\varepsilon_{fc} E_f \frac{A_f}{2} \leq 0.002 E_f \frac{A_f}{2}$	
Pre.7	[26]	$\beta_1 f_c' \, b \, c$		$\varepsilon_{fc} E_f \frac{A_f}{2} \leq 0.0035 E_f \frac{A_f}{2}$	

In contrast, the maximum limit of the compressive strain of the CFRP bars has been given as the concrete crushing strain, which is to be assumed as 0.003 [24-25] and 0.0035 [26]. This is due to the fact that the CFRP bars are anisotropic materials, which have lower compressive strength compared to their tensile strength. Additionally, CFRP bars cannot achieve their ultimate strengths like concrete can reach its crushing strain. Microsoft Visual Basic (vb.6) code was developed to find the axial load and moment resistance under eccentric loads and pure bending. The flowchart of the theoretical analysis procedure is presented in Figure 2. The process is initiated by assuming a certain value between $0.1h$ to h of the neutral axis position. Based on this assumption the strains in the tensile and compressive CFRP bars are calculated using the similarity of triangles with the assumptions of linear strain distribution, assuming 0.003 as the strain in the extreme concrete compressive fiber. The tensile strains are assumed to be negative, while the compressive strains are assumed to be positive. The stress in each layer of the CFRP bars was calculated with the help of the stress-strain relationships presented in Table II, and compared with the limits set in each used model.

TABLE III. DETAILS OF THE SPECIMENS

No.	Specimen ID	*e/h*	Type of reinforcement	Longitudinal bars	Ties
1	C10-T90-E0	0.0	CFRP	4Ø10 mm	Ø6 mm @ 90 mm
2	C10-T90-E0.5	0.5			
3	C10-T90-E1	1.0			
4	C12-T90-E0	0.0	CFRP	4Ø12 mm	Ø6 mm @ 90 mm
5	C12-T90-E0.5	0.5			
6	C12-T90-E1	1.0			
7	C16-T90-E0	0.0	CFRP	4Ø16 mm	Ø6 mm @ 90 mm
8	C16-T90-E0.5	0.5			
9	C16-T90-E1	1.0			
10	C12-T40-E0	0.0	CFRP	4Ø12 mm	Ø6 mm @ 40 mm
11	C12-T40-E0.5	0.5			
12	C12-T40-E1	1.0			
13	C12-T140-E0	0.0	CFRP	4Ø12 mm	Ø6 mm @ 140 mm
14	C12-T140-E0.5	0.5			
15	C12-T140-E1	1.0			

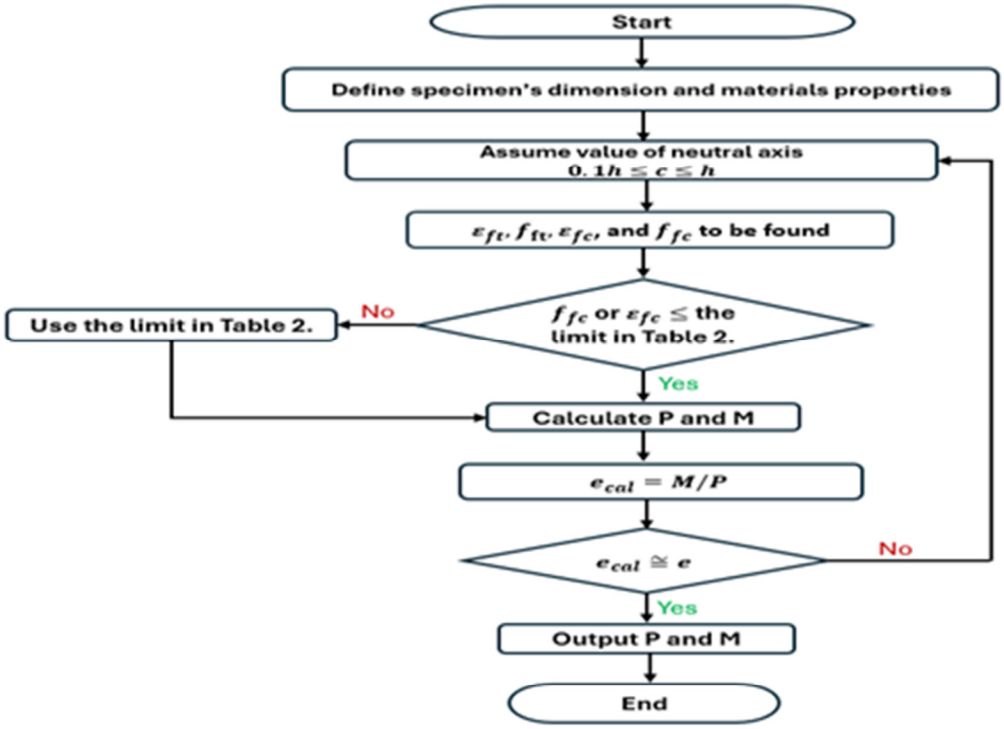

Fig. 2. Flowchart for theoretical analysis of CFRP-RC column.

The forces in the CFRP reinforcement were calculated as the product of stresses and the cross-sectional area of the bars. The axial load resistance is taken as the sum of the forces acting on the reinforcement and the forces acting on the concrete compressive section. Similarly, the bending moment resistance is taken as the sum of the moments of the centerline of the section under. The bending moment resistance is divided by the axial load resistance and equalized to the given eccentricity to check the assumed value of *c*.

IV. METHODOLOGY PROCESS

The experimental program presented in [16] was used to verify both the theoretical analysis and FEA. The test program involved a concrete column measuring 150 mm × 150 mm in cross-section and 1500 mm in height, with the mid-height test conducted at 900 mm. This short column has enlarged heads at both ends for eccentric load. The specimens were divided into five groups, as shown in Table III. Each group comprised three concrete columns with identical reinforcement details, tested under varying eccentricity conditions with *e/h* ratios of 0, 0.5, and 1. The specimen labels indicate the diameter of the CFRP bars, tie spacing, and the eccentricity of the load. For example, specimen C16-T90-E0.5 features four 16 mm diameter CFRP bars as longitudinal reinforcement, a tie spacing of 90 mm, and is tested under a 75 mm eccentric load (*e/h* = 0.5). The average concrete compressive strength was 44.7 MPa based on cylinder samples. The longitudinal reinforcements used CFRP bars measuring 10 mm, 12 mm, and 16 mm in diameter, while 6 mm diameter bars served as tie reinforcements, as detailed in Table IV.

TABLE IV. DETAILS OF USED CFRP PROPERTIES

Diameter (mm)	Area (mm^2)	Density (kg/m^3)	Tensile strength (MPa)	Modulus of elasticity (MPa)
6.0	28.0	1700	2000	148000
10	78.5			150000
12	113			145000
16	200			151000

V. EXPERIMENTAL, THEORETICAL, AND FEA RESULTS

This section presents CFRP-RC columns' experimental, theoretical, and FEA results. The experimental results from [16] were adopted, while seven different analytical methods were employed to evaluate the theoretical contribution of the CFRP bars in the compression zone. For the FEA, the specimens were simulated until failure, with each specimen reaching its maximum load capacity. Tables V and VI present the FEA and theoretical results of the load-carrying capacity, the stresses in the longitudinal bars, and the lateral and axial displacements of the tested specimen. The failure modes and mechanisms were influenced by eccentricity. However, the failure of the CFRP-RC columns was not caused by bar rupture on either the tension or compression sides. Furthermore, the results demonstrated good agreement with the experimental data reported in [16]. The concentric-loaded specimens, depicted in Figure 3, displayed a failure mode characterized by a sudden and explosive nature, resulting from concrete crushing before the CFRP bars attained their ultimate strength.

As all tested specimens were under compressive stress, the cracks needed a higher compressive load to initiate. Cracks started to appear when the load reached 49%-69% of the applied load. Before failure, there were visible cracks on the specimens at both the top and bottom ends. All specimens exhibited no vertical crushing except for C12-T140, where vertical cracks developed at 52% of the failure load, as seen in Figure 3(a). As the load on the columns progressively increased, these vertical cracks progressively multiplied and widened. In all tested specimens, the stress concentrations near the column ends caused crushing of the concrete cover. The tested specimens exhibited compressive failure modes.

For specimens loaded with moderate and extreme eccentricity (e/h = 0.5 and 1), the eccentric load caused the specimens to bend, leading to compression on one side and tension on the other, as evidenced in Figures 4 and 5. When the applied tensile stress reached the concrete's tensile strength capacity, flexural tension cracks appeared on the tension side of the CFRP-RC columns at about 32%-28% of the maximum load. As the load increased, these cracks expanded, and additional parallel cracks formed along the column's height, extending toward the neutral axis and resulting in the failure of the compression concrete block. Increasing eccentricity from zero to extreme had a substantial effect on the overall performance, including the ultimate capacity, which was reduced by 69%-87%, when with the concentric-loaded specimens. Overall, the specimens tested under moderate eccentricity exhibited flexural-compression failure.

TABLE V. EXPERIMENTAL RESULTS: LOAD CAPACITY, MOMENT, AND DISPLACEMENTS UNDER VARYING ECCENTRICITY (e/h)

NO.	specimen	ρ%	e/h	P (kN)	e (mm)	U_{lat} (mm)	M_{1st} (kN.m)	M_{2nd} (kN.m)	MT (kN.m)	U_{axial} (mm)	μ
1	C10-T90	1.40	0.00	892	0.00	2.40	0.00	2.14	2.14	4.05	14.64
2			0.25	533	37.50	4.36	19.99	2.32	22.31	2.19	7.70
3			0.50	262	75.00	15.40	19.65	4.03	23.68	1.83	5.46
4			0.75	155	112.50	15.79	17.44	2.45	19.88	1.93	4.84
5			1.00	126	150.00	19.80	18.90	2.49	21.39	2.41	4.67
6	C12-T90	2.00	0.00	939	0.00	4.00	0.00	3.76	3.76	5.15	11.43
7			0.25	562	37.50	4.30	21.08	2.42	23.49	2.76	9.57
8			0.50	285	75.00	15.50	21.38	4.42	25.79	2.30	8.95
9			0.75	182	112.50	17.20	20.48	3.13	23.61	2.19	7.74
10			1.00	135	150.00	17.60	20.25	2.38	22.63	3.07	6.67
11	C16-T90	3.57	0.00	1104	0.00	1.57	0.00	1.73	1.73	4.00	8.48
12			0.25	592	37.50	4.33	22.20	2.56	24.76	1.67	7.90
13			0.50	326	75.00	16.30	24.45	5.31	29.76	1.30	6.75
14			0.75	232	112.50	17.60	26.10	4.08	30.18	0.80	6.09
15			1.00	167	150.00	19.20	25.05	3.21	28.26	1.53	5.25
16	C12-T40	2.00	0.00	930	0.00	2.96	0.00	2.75	2.75	3.70	13.27
17			0.25	580	37.50	4.20	21.75	2.44	24.19	2.55	11.00
18			0.50	272	75.00	13.50	20.40	3.67	24.07	1.44	7.38
19			0.75	187	112.50	16.80	21.04	3.14	24.18	1.27	6.87
20			1.00	119	150.00	17.20	17.85	2.05	19.90	1.25	6.38
21	C12-T140	2.00	0.00	915	0.00	2.70	0.00	2.47	2.47	7.07	17.57
22			0.25	535	37.50	5.66	20.06	3.03	23.09	1.97	11.29
23			0.50	284	75.00	14.60	21.30	4.15	25.45	2.38	9.24
24			0.75	184	112.50	15.60	20.70	2.87	23.57	2.11	8.95
25			1.00	127	150.00	16.20	19.05	2.06	21.11	3.35	7.22

By increasing eccentricity to a high level, the response closely resembled that of the flexural members. The lateral deflection at mid-height of the tested column is an indication of column stiffness. For all tested columns (Figure 6), the early crack initiation on the tension side under eccentric loading led to significant reductions in the both axial and lateral stiffness. For this reason, the slope of the load-deflection curves was inversely proportional with the eccentricity level, while the deflection at failure load was directly proportional. The test results illustrated in Table V and the load-deflection curves depicted in Figure 6 indicate that the eccentricity plays a remarkable role in the axial capacity and stiffness of the columns. Finally, the FEA results were compared with the experimental results for the RC columns with steel reinforcement. It can be noticed that the CFRP-reinforced columns showed a lesser slope than the steel-reinforced columns due to the higher modulus of elasticity of the steel reinforcement, which affected the stiffness of the tested specimens. Ductility measures a material's capability to undergo notable plastic deformation without noticeable fracturing. According to [27], ductility can be explained as the ductility index determined by the ratio of the axial deflection corresponding to 85% of the ultimate load capacity to the axial deflection corresponding to the yield limits (elastic limits).

Table V includes the calculated ductility indexes (μ) for all specimens analyzed in the FEA study. Compared to the experimental results from [16] for the steel-reinforced specimens, it can be observed that the CFRP-RC specimens showed higher ductility than the steel-RC specimens. This behavior occurs because, at ultimate load, the CFRP bars had not reached their ultimate tensile strain, unlike the steel reinforcement, which typically yields to failure. This suggests that CFRP-reinforced columns may sustain additional loads and deformations beyond ultimate load. The same observation was reported in [9, 28-29].

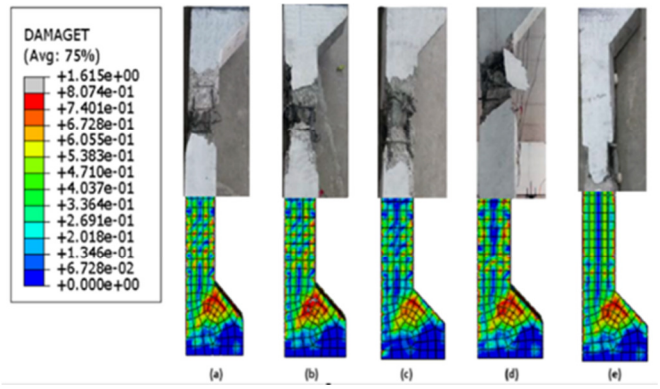

Fig. 3. Failure mode of columns tested under concentric load: (a) C10-T90, (b) C12-T90, (c) C16-T90,(d) C12-T40, (e) C12-T140.

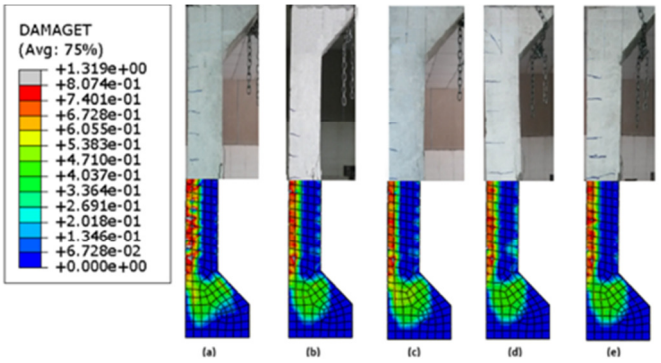

Fig. 4. Failure mode of columns tested under load with moderate eccentricity (e/h =0.5): (a) C10-T90, (b) C12-T90, (c) C16-T90, (d) C12-T40, (e) C12-T140.

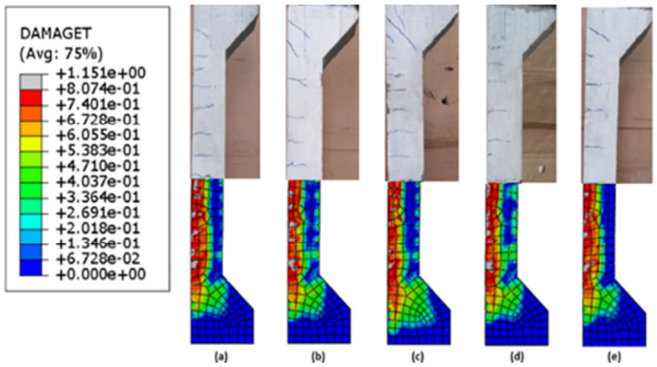

Fig. 5. Failure mode of columns tested under load with extreme eccentricity (e/h =1): (a) C10-T90, (b) C12-T90, (c) C16-T90, (d) C12-T40, (e) C12-T140.

From Table V, it can be noticed that the specimens with high eccentricity were more ductile compared to the specimens under load with small eccentricities. This is consistent with [28, 30], where it was demonstrated that the FRP-RC columns had low ductility at a low eccentricity level and as the eccentricity level increased, the improvement in ductility became noticeable. The observed reduction in specimen ductility with an increased CFRP reinforcement ratio is attributed to the enhanced strength provided by additional longitudinal reinforcement. Conversely, ductility improved with a reduced transverse reinforcement spacing due to more effective confinement.

In the theoretical analysis, calculating the stresses in the CFRP bars is necessary to find the axial and bending resistance of the column. By assuming a linear strain distribution, the strain data from the CFRP reinforcement in compression and tension were analyzed to establish the theoretical neutral axis at different eccentricity levels, as shown in Figure 7(a). It is also worth noting that the theoretical values were calculated based on the principle of balance and the assumptions of the contribution of the CFRP bars lying in the compression zone, which were adopted in each model. Figure 7 shows that the FE model gives higher values for the neutral axis than the theoretical models, but with good agreement, it reached to 16%. For the theoretical models, the concrete contribution (concrete compressive strength and column cross-section) in the calculation of axial resistance has a superior effect on the neutral axis values. The first predicted equation (Pre.1) gives higher values than other models since the contribution of the CFRP bars' effect was ignored, i.e., only the concrete will balance the CFRP bars in the tension zone. In comparison, lower values can be noticed from Pre. 6 due to the higher contribution of concrete resistance (assuming b_1 as 0.9). The same amount of concrete contribution in predicted equations (Pre. 2, 3, 4, and 5) gives the same values for the neutral axis position.

FEA and theoretical results indicated that the CFRP reinforcement developed significant compression and tension stresses, confirming its role in sustaining various eccentric forces. The stresses were recorded at the mid height level, where the maximum compression and tension stresses were expected. Table VI illustrates the average stresses recorded for the CFRP bars lying in the compression and tension zones at the peak load, for the theoretical analysis and FEA, as well as for different eccentricity levels (e/h = 0 to pure bending). It can be noticed that for all specimens and for all considered methods, when e/h = 0, only compression stresses were generated because the neutral axis is equal to the column depth. FEA gives higher values compared to the theoretical methods since the stresses are allowed to reach their maximum possible limit (f_{yt}). For specimen C10-T90, at peak load, the FEA compression stresses range from -684 MPa to -117 MPa with a contribution up to 34.2% and 5.8% of the bar's ultimate tensile stress (f_{yt} = 2000 MPa) for the range of eccentricities e/h = 0 to pure bending, respectively. The tensile stresses for the same specimen were 0-711 MPa, with a contribution up to 0% and 35.5% of the bar's ultimate tensile stress.

Regarding the theoretical methods, the first method ignores the contribution of the CFRP bars in compression compared with other methods. The predicted methods: Pre. 2, 3, 4, and 5 have approximately similar values of compression and tension stresses for the full range of eccentricities due to the same predicted values of C (position of neutral axis), and differ when e/h = 0. In both FEA and the theoretical analysis, increasing the CFRP reinforcement ratio affects the stress values since the bar diameter and the elastic modulus are contributing in calculating the neutral axis's position.

(a) (b)

Fig. 6. Load versus deflection: (a) lateral deflection, (b) axial deflection.

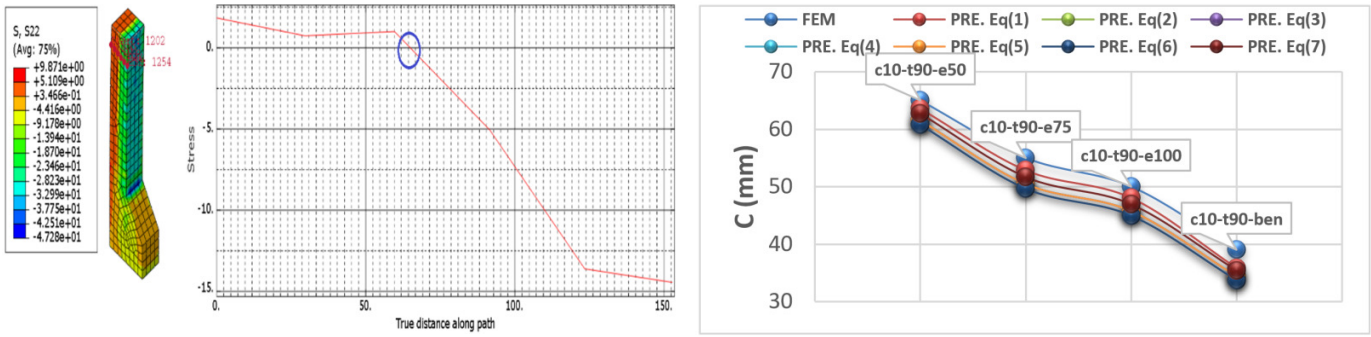

(a) (b)

Fig. 7. FEA and theoretical values of neutral axis position: (a) neutral axis as presented in Abaqus, (b) specimen C10-T90.

In FEA, changing the arrangement of the lateral reinforcement (adjusting the spacing of ties) affects the stress contribution in both tension and compression by 29%-32%, unlike the theoretical analysis, which ignores the effects of the lateral confinement. When the range of eccentricity is small (e/h = 0.25), all CFRP bars exhibited compressive stresses in FEA, contrasting with the theoretical predictions. This discrepancy arises because the neutral axis position at these eccentricities extends beyond the bars' centerline in the compression zone, resulting in larger neutral axis values than anticipated.

The contribution of the CFRP at the peak axial load is shown in Table VII. For each specimen, the axial stress in the four longitudinal CFRP bars (F_{fc1} to F_{fc4}) was recorded, as portrayed in Figure 8, and the average axial stress (F_{fc}) was calculated. The total load supported by the CFRP bars was obtained by multiplying the average axial stress by the total cross-sectional area of the bars. Finally, the contribution of the CFRP bars to the peak axial load was determined by calculating the ratio of the load carried by the CFRP bars to the total load sustained by the entire specimen. Each theoretical model used in this study has already determined the maximum stress or strain limits of the CFRP bars lying in the compression zone. It was found that the FE model gives higher values of the CFRP bar contribution compared with other theoretical models, ranging from 24% to 61%. For the theoretical models, the predicted model (Pre.2) gives higher contribution values than other models as a high contribution assumption value ($0.35F_{yt}$) is utilized. The CFRP bars' contribution to the other models ranges from 10% to 36%. It is also worth noting that the model Pre.1 ignores any contribution of the CFRP bars to the peak axial resistance. Increasing the CFRP reinforcement ratio increases the contribution by 15%-43%, 6%-19%, and 7%-20%, for FEA, Pre.2, and Pre.7, respectively. Similar an increase can be noticed for Pre.3 and Pre.6, which range from 4% to 13%, and for Pre.4 and Pre.5, ranging from 5% to 17%, due to the similarity of the contribution assumptions. In the theoretical model, it can be noticed that changing the distribution of lateral reinforcement (adjusting the spacing of ties) did not affect the contribution ratio because the effect of confinement is ignored in all theoretical models, unlike the FEA, which gives higher contribution values due to the higher stresses sustained by the bars with smaller spacing of ties. Generally, the total bending moment capacity, given by (14), of the tested specimens at the failure stage was composed of first-order moments (M_1), resulting from the initial applied eccentricity, and second-order moments (M_2) due to the second-order effects. The second order refers to the nonlinear effects, which show an additional moment as a product of the axial load at the failure point by the corresponding lateral deflection. Generally, the value of the second-order moment is governed by the initial eccentricity and the column's slenderness. When the load is applied with an initial eccentricity, an increase in the mid-height deflection is caused. Having introduced an initial load eccentricity increased the column's mid-height deflection, leading to the possibility of a second-order effect. However, having followed the increase of this initial eccentricity, a decrease in the axial load resistance caused a reduction in the second-order bending moment. In other words, applying a higher eccentricity level may not always give an increase in the second-order moment.

$$M = M_1 + M_2 \quad (14)$$

As shown in Figures 9 and 10, the ratio of M_2/M_1 was at its highest in CFRP-RC columns when the column was loaded with a moderate eccentricity, and then the ratio declined when the eccentricity increased. The reason for this behavior is the balance between the axial resistance and lateral deflection at a moderate eccentricity level, unlike in higher eccentricity levels, where despite the increase in lateral deflection, the axial resistance decreased considerably. For FEA, the M_2/M_1 ratio for the CFRP-RC specimens labeled C12-T90 and tested under moderate and high eccentric loading was 21% and 12%.

Regarding the experimental ratio for the same level of eccentricity, it results in the axial resistance of 24%, and 12.1%. However, in RC columns reinforced with steel bars, this ratio approximately decreased by 11% for the moderate level and increased by 7% for a higher level. It can be, thus, concluded that CFRP-RC columns were subjected to greater second-order effects than the steel-RC columns due to the low modulus of elasticity of the CFRP bars. Also, these results show good agreement with the experimental findings reported in [31].

TABLE VI. FE AND THEORETICAL STRESSES FOR CFRP BARS IN TENSION AND COMPRESSION ZONES

Specimen	e/h	FE		Pre.1		Pre.2		Pre.3		Pre.4		Pre.5		Pre.6		Pre.7	
		F_{ft}	F_{fc}	F_{ft}	F_{fc}	F_{ft}	F_{fc}	F_{ft}	F_{fc}	F_{ft}	F_{fc}	F_{ft}	F_{fc}	F_{ft}	F_{fc}	F_{ft}	F_{fc}
C10-T90	0.00	-684		-		-700		-300		-450		-450		-300		-525	
	0.25	-31	-361	126		115	-332	115	-300	115	-332	115	-332	118	-300	111	-332
	0.50	278	-328	428		456	-260	456	-260	456	-260	456	-260	468	-258	439	-264
	0.75	337	-245	606		655	-218	655	-218	655	-218	655	-218	673	-214	629	-224
	1.00	456	-156	711		769	-194	769	-194	769	-194	769	-194	791	-190	739	-201
	bending	566	-117	1106		1172	-110	1172	-110	1172	-110	1172	-110	1204	-103	1126	-120
C12-T90	0.00	-813		-		-700		-290		-435		-435		-29-		-508	
	0.25	-32	-238	110		98	-330	99	-290	98	-330	98	-330	101	-300	94	-331
	0.50	189	-213	352		384	-267	384	-267	348	-267	348	-267	395	-265	370	-270
	0.75	291	-174	490		546	-231	546	-231	546	-231	546	-231	562	-228	525	-236
	1.00	388	-118	573		640	-211	640	-211	640	-211	640	-211	658	-207	615	-216
	bending	682	-111	887		972	-138	972	-138	972	-138	972	-138	999	-132	935	-146
C16-T90	0.00	-928		-		-700		-302		-453		-453		-302		-529	
	0.25	-36	-265	85		71	-325	72	-302	71	-325	71	-325	75	-300	68	-326
	0.50	149	-249	254		293	-272	293	-272	293	-272	293	-272	301	-270	282	-275
	0.75	239	-234	346	-	412	-244	412	-244	412	-244	412	-244	423	-241	396	-247
	1.00	308	-197	402		480	-227	480	-227	480	-227	480	-227	493	-224	462	-231
	bending	622	-102	616		726	-168	726	-168	726	-168	726	-168	745	-164	700	-174
C12-T40	0.00	-837		-		-700		-290		-453		-453		-290		-508	
	0.25	-33	-250	110		98	-330	99	-290	98	-330	98	-330	101	-300	94	-331
	0.50	200	-241	352		384	-267	384	-267	348	-267	348	-267	395	-265	370	-270
	0.75	312	-177	490		546	-231	546	-231	546	-231	546	-231	562	-228	525	-236
	1.00	329	-140	573		640	-211	640	-211	640	-211	640	-211	658	-207	615	-216
	bending	485	-136	887		972	-138	972	-138	972	-138	972	-138	999	-132	935	-146
C12-T140	0.00	-767		-		-700		-290		-453		-453		-290		-508	
	0.25	-35	-263	110		98	-330	99	-290	98	-330	98	-330	101	-300	94	-331
	0.50	181	-253	352		384	-267	384	-267	348	-267	348	-267	395	-265	370	-270
	0.75	251	221	490		546	-231	546	-231	546	-231	546	-231	562	-228	525	-236
	1.00	380	-207	573		640	-211	640	-211	640	-211	640	-211	658	-207	615	-216
	bending	731	-185	887		972	-138	972	-138	972	-138	972	-138	999	-132	935	-146

TABLE VII. COMPRESSION CONTRIBUTION OF CFRP BARS TO THE AXIAL RESISTANCE

Specimens		C10-T90-e0	C12-T90-e0	C16-T90-e0	C12-T40-e0	C12-T140-e0
P_{fc} (kN)	FEM	215	367	742	378	-
	Pre.2	220	316	560	316	316
	Pre.3	94.0	131	242	131	131
	Pre.4	141	197	362	197	197
	Pre.5	141	197	362	197	197
	Pre.6	94.0	131	242	131	131
	Pre.7	165	229	423	229	229
P (kN)	FEM	892	939	1104	930	915
	Pre.2	1063	1154	1387	1154	1154
	Pre.3	937	969	1066	969	969
	Pre.4	984	1034	1186	1034	1034
	Pre.5	984	1034	1186	1034	1034
	Pre.6	987	1018	1114	1018	1018
	Pre.7	1009	1009	1181	1009	941
% of CFRP bars contribution	FEM	24	39	67	41	38
	Pre.2	21	27	40	27	27
	Pre.3	10	14	23	14	14
	Pre.4	14	19	31	19	20
	Pre.5	14	19	31	19	20
	Pre.6	10	14	23	14	14
	Pre.7	16	23	36	23	24

P_{fc} is axial load sustained by CFRP bars in the compression zone

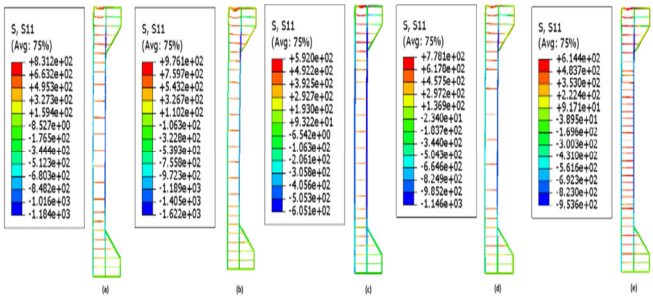

Fig. 8. Axial stress in CFRP bars for specimens: (a) C10-T90, (b) C12-T90, (c) C16-T90, (d) C12-T40, (e) C12-T140.

The diagrams were compared with the experimental results in [16]. For generating the FEA and theoretical P-M interaction diagram, the axial load resistance and cross-pounding bending moment resistance were determined for 6 different points, with different eccentricity levels starting from the point of the axial load resistance when the specimen is under concentric applied load (e/h = 0), low eccentricity level (e/h = 0.25), moderate level (e/h = 0.5), high level (e/h = 0.75), extreme level (e/h = 1), and ending with the point of pure bending. From these results as well as K_n and R_n, the normalized P-M interaction diagrams were developed. K_n and R_n were calculated using:

$$K_n = \frac{P}{A_g f'_c} \quad (15)$$

$$R_n = \frac{M}{A_g f'_c h} \quad (16)$$

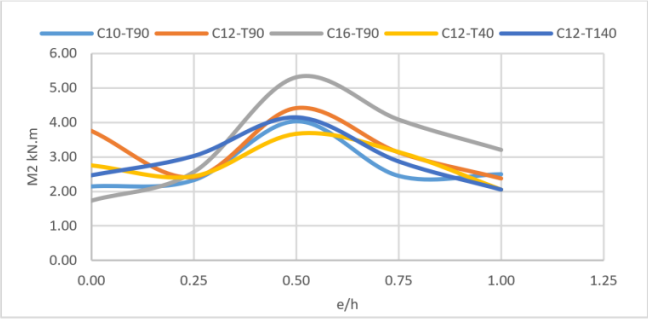

Fig. 9. Second-order moment versus eccentricity level.

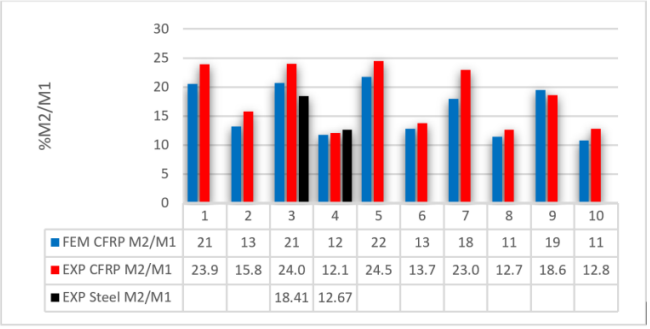

	1	2	3	4	5	6	7	8	9	10
FEM CFRP M2/M1	21	13	21	12	22	13	18	11	19	11
EXP CFRP M2/M1	23.9	15.8	24.0	12.1	24.5	13.7	23.0	12.7	18.6	12.8
EXP Steel M2/M1			18.41	12.67						

Fig. 10. Effect of reinforcement type on second-order moment.

In FEA, the bending moment resistance (M) was combined with the bending moment due to load eccentricity and the bending moment due to mid-height lateral deflection. As the lateral deflection in the theoretical calculation was ignored, the bending moment due to load eccentricity was dominated. Figure 11 presents the P-M interaction diagrams for the specimen C10-T90. Under zero eccentricity level, the FE model exhibited higher axial resistance and lower bending resistance by 5% and 50% compared with the experimental results. Similar results can be noticed for moderate eccentricity levels. High-level eccentricity gives higher FEA axial resistance by 6% and lower bending resistance by 6%, as shown in Figure 13(a). Neglecting the compressive contribution of the CFRP bars (as in model Pre.1) results in a 15% underestimation of the axial resistance at low eccentricity and an 8% underestimation at moderate eccentricity, with negligible effects at high and extreme eccentricity levels. The bending moment resistance decreased by nearly the same amount, which is 21% for all points except the pure bending point in which ignoring the CFRP contribution in compression increases the bending moment resistance by 20%. However, the interaction diagram developed in this predicted method lies below both the experimental and FEA diagrams, but with a slightly good agreement. As previously discussed, the theoretical model proposed in [13] accounts for CFRP bars' compressive contribution, limiting it to a maximum of 35% of their ultimate tensile strength. The predicted P-M interaction diagram in Figure 12(a) lies below both the experimental and FEA results, though, it shows a generally good agreement with the FEA data. A significant improvement in resistance was observed, with a 19% increase in the pure axial capacity and a 30% enhancement in the pure bending moment capacity.

The compressive contribution of the CFRP bars can be quantified via the strain and elastic modulus, as implemented in models Pre.3 and Pre.6. These models share identical CFRP contribution assumptions but differ in concrete compressive strength terms: Pre.3 uses $0.85f'_c$, while Pre.6 adopts $0.9f'_c$. For both predicted models, the bending resistances in different eccentricity levels were found to be lower by 13% when compared with the experimental and FEA results. Like other predicted models, an improvement in bending resistance can be noticed at the point of pure bending and it reaches 30% compared to the FEA results, Also, Pre.6 gives higher interaction values for the full range of eccentricities compared with Pre.3 due to the higher contribution of concrete. The theoretical results underestimate the CFRP contribution compared to the FEA results, except for the points of pure axial and pure bending. Both models improved the axial resistance by 5% for Pre.3.

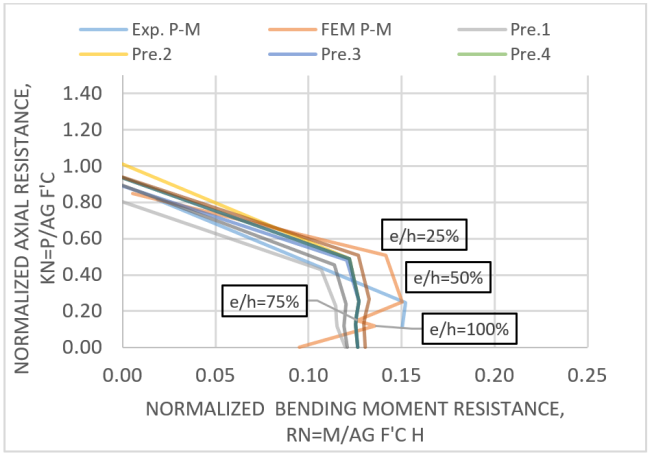

Fig. 11. Interaction diagrams for specimen C10-T90.

Using an unconfined concrete strain of 0.003 and multiplying by the elastic modulus, both model Pre.4 [24] and model Pre.5 [24] yielded identical results for CFRP contribution, as shown in Figure 12(c). The improvement in the axial resistance at the full range of eccentricity did not exceed 16% and 10% compared with the experimental and FEA results, respectively, also with a 30% improvement in pure bending. The last theoretical model (Pre.7) presented in [26] decreased the contribution of the concrete compressive strength and replaced the loss in the contribution by increasing the contribution of the CFRP bars. This increase was achieved by limiting the CFRP strain to a maximum value of 0.0035. For pure axial bending, an increase of 6% and 11% was noticed compared with the FEA and experimental results. This improvement indicates a decrease in the axial resistance to low and moderate levels of eccentricity. In the bending resistance, the predicted model and the whole eccentricity levels give lower values reaching 26% based on the FEA results, while the predicted model remains superior in calculating the pure bending moment resistance compared to the FE model by 20%, as shown in Figure 12(d). Figure 13 presents the P-M interaction diagrams for experimental, FE analysis, and all theoretically predicted models used in this study.

The study also examined the effects of varying transverse reinforcement spacing, with configurations of 140 mm (increased spacing) and 40 mm (reduced spacing). Three longitudinal CFRP reinforcement ratios were investigated: 1.4%, 2.0%, and 3.57%. The P-M interaction diagram for various reinforcement ratios and tie spacing are displayed in Figure 12. It can be noticed that increasing the CFRP reinforcement ratio from 1.4% to 2% and 3.57% increases the pure axial resistance by 5% and 23%, respectively. When the eccentricity level increased, the improvement in the axial resistance, due to the increasing CFRP reinforcement ratio, increased by 13% for a ratio of 2% and 33% for a ratio of 3.57%. The bending resistance increased proportionally with the reinforcement ratio, and the most noticeable improvement can be seen at the point of pure bending, which reached 60% for a ratio of 2% and 141% for a ratio of 3.57%. In FEA, changing the tie spacing has a slight effect on the axial resistance along the full range of eccentricity levels, while a remarkable decrease (12.6%) in bending resistance can be observed at the point of pure bending, when the tie spacing decreases from 90 mm to 40 mm. According to [25, 32], decreasing the tie spacing affects significantly the failure mode of the tested specimen due to the generation of a separate plane between the specimen core and the outside concrete cover, causing the fall of the concrete cover as well as that of the specimen.

In the theoretical models, the tie spacing variations show no effect since the transverse reinforcement contributions are excluded from the P-M interaction calculations. When the compressive strength of the CFRP is ignored, the increase in the reinforcement ratio causes a decrease in the axial resistance. For e/h = 0, increasing the reinforcement ratio from 1.4% to 2% and 3.57% decreases the axial resistance by 0.8% and 2%, respectively. This decrease in the axial resistance is attributed to the subtraction of a larger reinforcing area from the specimen's total area in the calculation. With an increasing eccentricity level, any increase in the reinforcement ratio causes an increase in the neutral axis value, which gives a higher concrete contribution in axial resistance. The axial resistance improvement for the ratio of 2% starts from 0.8% for the low eccentricity level and reaches 9% for the extreme level, while for the reinforcement ratio of 3.57%, the improvement reaches 22% for the extreme level of eccentricity. Similarly, the bending resistance improved by 0.9%-11%, and 2%-29% for reinforcement ratios of 2% and 3.57%, respectively.

Figure 13 illustrates the effects of considering the CFRP compressive strength contribution in addition to increasing the CFRP reinforcement ratio on the axial and bending resistances. The improvement in pure axial resistance ranged from 8% to 30% for reinforcement ratios of 2% and 3.57%, respectively. This improvement was due to the higher compression stress (700 MPa) in CFRP bars. In a low eccentricity level (e/h = 25%), the compression stress value decreased by 53% due to a decrease in the neutral axis values, while the overall decrease in the axial resistance was 5% and 18%.

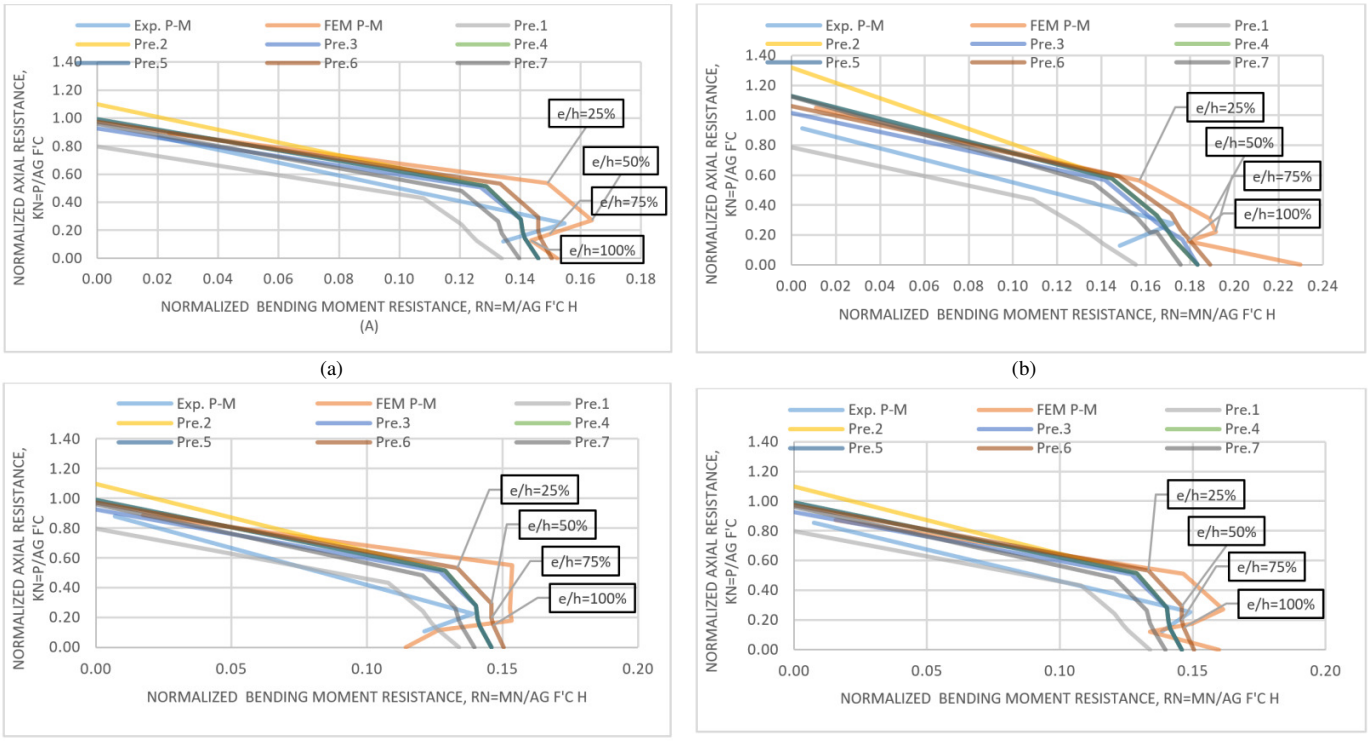

(a) (b)

(c) (d)

Fig. 12. Experimental, FEA, and theoretical interaction diagrams for specimens: (a) C12-T90, (b) C16-T90, (c) C12-T40, (d) C12 T140.

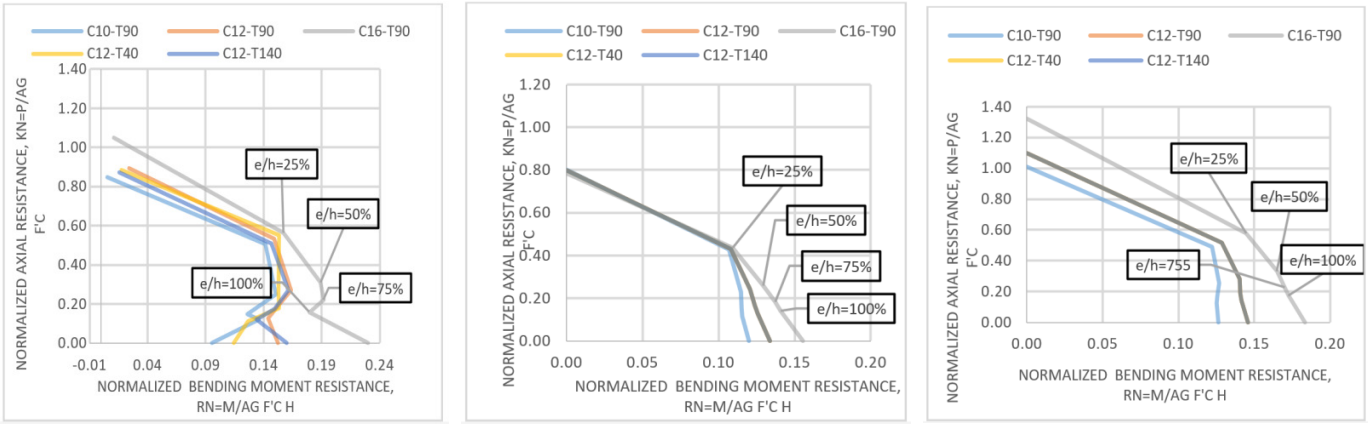

(a) (b) (c)

Fig. 13. Contribution effect of CFRP bars on interaction diagrams for all specimens: (a) FEA, (b) model Pre.1, (c) model Pre.2.

For moderate (e/h = 0.5), high (e/h = 0.75), and extreme (e/h = 1.0) eccentricity levels, increasing the reinforcement ratio from 2% to 3.57% enhanced the axial resistance by 10%-29%, 12%-35%, and 18%-38%, respectively. With the increase in the eccentricity level until the pure bending point, the improvement in bending resistance was in line with the increase in the reinforcement ratio by 5%-15% for a 2% reinforcement ratio, while for a 3.57% reinforcement ratio, the improvement ranged from 18% to 45%. Finally, the P-M interaction diagrams for the columns reinforced with CFRP do not show any balanced points, in contrast to the diagrams for the columns reinforced with steel. Additionally, in all cases, the CFRP bars did not fail under tension or compression, even when the concrete reached its ultimate strain, which is assumed to be 0.003. As the reinforcement ratio increased, the strains in the tensile bars under pure bending conditions decreased.

VI. CONCLUSIONS

This study provides insights into the behavior of Carbon Fiber-Reinforced Polymer-Reinforced Concrete (CFRP-RC) columns under varying loading conditions. The structural behavior of rectangular concrete columns reinforced with CFRP bars under concentric and eccentric loaded conditions was investigated. Based on the Finite Element Analysis (FEA), and theoretical results, the following observations were made:

1. The CFRP-RC columns can be potentially analyzed by deploying the procedure used for traditional RC columns with steel reinforcement.
2. The FEA observations indicate that no rupture in the CFRP bars lies in the tension zone, and the failure is triggered by concrete crushing. For the tested columns, the failure mode can be classified as a brittle compression failure for zero and low eccentricity levels. However, for specimens with moderate, high, and extreme eccentricities, a less brittle flexural–compression failure can be noticed, and the response closely resembled that of the flexural members as the eccentricity ratio increased.
3. Compared to the concentric specimens, FEA demonstrates an average decrease in initial stiffness by 43%, 89%, 92%, and 94% for low, moderate, high, and extreme eccentric loading levels, respectively. Additionally, for all specimens, regardless of the longitudinal reinforcement ratio or transverse reinforcement configuration, the ductility index demonstrates an inverse relationship with the eccentricity level.
4. In FEA, the CFRP reinforcement can be used as an internal reinforcement by limiting its ultimate tensile strength to a suitable fraction.
5. Increasing the reinforcement ratio enhances the axial capacity by 33% and increases the bending resistance by 141%. Modifying the spacing of ties from 140 mm to 40 mm has little effect on the axial capacity. However, a decrease in the tie spacing results in a reduction of the bending resistance.
6. Given the limited understanding of CFRP bars' compressive behavior in high-strength concrete, further investigations are required.
7. Finally, unlike the traditional steel-RC columns, the obtained P-M interaction diagrams of the CFRP reinforced columns do not experience balanced points.

REFERENCES

[1] *Building code requirements for structural concrete reinforced with glass fiber-reinforced polymer (GFRP) bars-code and commentary: an ACI Standard*, ACI 440.11-22, American Concrete Institute, Farmington Hills, MI, Sep. 2022.

[2] *Standard Test Method for Tensile Properties of Fiber Reinforced Polymer Matrix Composite Bars*, ASTM D7205, ASM International, West Conshohocken, Pennsylvania, Dec. 2011.

[3] *Design and construction of building components with fiber reinforced polymer*, CAN/CSA S806-12, Canadian Standards Association, Rexdale, ON, Canada, 2012.

[4] Q. Khan, M. N. Sheikh, and M. N. S. Hadi, "Tension and compression testing of Fibre Reinforced Polymer (FRP) bars," in *Joint Conference of the 12th Int. Symp. on Fiber Reinforced Polymers for Reinforced Concrete Structures and the 5th Asia-Pacific Conference on Fiber Reinforced Polymers in Structures*, Nanjing, China, Dec. 2015, pp. 1–6.

[5] G. B. Maranan, A. C. Manalo, B. Benmokrane, W. Karunasena, and P. Mendis, "Behavior of concentrically loaded geopolymer-concrete circular columns reinforced longitudinally and transversely with GFRP

bars," *Engineering Structures*, vol. 117, pp. 422–436, Jun. 2016, https://doi.org/10.1016/j.engstruct.2016.03.036.

[6] W. Xue, F. Peng, and Z. Fang, "Behavior and Design of Slender Rectangular Concrete Columns Longitudinally Reinforced with Fiber-Reinforced Polymer Bars," *ACI Structural Journal*, vol. 115, no. 2, Mar. 2018, https://doi.org/10.14359/51701131.

[7] L. Al-Najmi and F. Abed, "Evaluation of FRP Bars under Compression and Their Performance in RC Columns," *Materials*, vol. 13, no. 20, Oct. 2020, Art. no. 4541, https://doi.org/10.3390/ma13204541.

[8] H. Tobbi, A. H. Farghaly, and B. Benmokrane, "Behavior of Concentrically Loaded Fiber-Reinforced Polymer Reinforced Concrete Columns with Varying Reinforcement Types and Ratios," *ACI Structural Journal*, vol. 111, no. 2, Mar. 2014, https://doi.org/10.14359/51686528.

[9] H. M. Mohamed, M. Z. Afifi, and B. Benmokrane, "Performance Evaluation of Concrete Columns Reinforced Longitudinally with FRP Bars and Confined with FRP Hoops and Spirals under Axial Load," *Journal of Bridge Engineering*, vol. 19, no. 7, Jul. 2014, Art. no. 04014020, https://doi.org/10.1061/(ASCE)BE.1943-5592.0000590.

[10] A. Hadhood, H. M. Mohamed, and B. Benmokrane, "Axial Load–Moment Interaction Diagram of Circular Concrete Columns Reinforced with CFRP Bars and Spirals: Experimental and Theoretical Investigations," *Journal of Composites for Construction*, vol. 21, no. 2, Apr. 2017, Art. no. 04016092, https://doi.org/10.1061/(ASCE)CC.1943-5614.0000748.

[11] S. El-Gamal and O. Al-Shareedah, "Behavior of axially loaded low strength concrete columns reinforced with GFRP bars and spirals," *Engineering Structures*, vol. 216, Aug. 2020, Art. no. 110732, https://doi.org/10.1016/j.engstruct.2020.110732.

[12] M. Z. Afifi, H. M. Mohamed, and B. Benmokrane, "Strength and Axial Behavior of Circular Concrete Columns Reinforced with CFRP Bars and Spirals," *Journal of Composites for Construction*, vol. 18, no. 2, Apr. 2014, Art. no. 04013035, https://doi.org/10.1061/(ASCE)CC.1943-5614.0000430.

[13] H. Tobbi, A. H. Farghaly, and B. Benmokrane, "Concrete columns reinforced longitudinally and transversally with glass fiber-reinforced polymer bars," *ACI Structural Journal*, vol. 109, no. 4, pp. 551–558, Jul. 2012.

[14] X. Fan and M. Zhang, "Behaviour of inorganic polymer concrete columns reinforced with basalt FRP bars under eccentric compression: An experimental study," *Composites Part B: Engineering*, vol. 104, pp. 44–56, Nov. 2016, https://doi.org/10.1016/j.compositesb.2016.08.020.

[15] J. Youssef and M. N. S. Hadi, "Axial load-bending moment diagrams of GFRP reinforced columns and GFRP encased square columns," *Construction and Building Materials*, vol. 135, pp. 550–564, Mar. 2017, https://doi.org/10.1016/j.conbuildmat.2016.12.125.

[16] Z. S. Othman and A. H. Mohammad, "Behaviour of Eccentric Concrete Columns Reinforced with Carbon Fibre-Reinforced Polymer Bars," *Advances in Civil Engineering*, vol. 2019, no. 1, Jan. 2019, Art. no. 1769212, https://doi.org/10.1155/2019/1769212.

[17] B. R. Hassan and A. R. Yousif, "Experimental and Analytical Investigation of Shear Behavior and Strength of Haunched Beams Reinforced with Basalt Fiber–Reinforced Polymer Rebars," *Journal of Bridge Engineering*, vol. 29, no. 12, Dec. 2024, Art. no. 04024098, https://doi.org/10.1061/JBENF2.BEENG-6723.

[18] H. M. Salman and M. H. Al-Sherrawi, "M-N Interaction Diagrams of RC Columns Strengthened with Steel C-Sections and Battens," *Civil Engineering Journal*, vol. 10, no. 6, pp. 1974–1986, Jun. 2024, https://doi.org/10.28991/CEJ-2024-010-06-016.

[19] K. H. Yang, J. H. Mun, M.-S. Cho, and T. H.-K. Kang, "Stress-Strain Model for Various Unconfined Concretes in Compression," *ACI Materials Journal*, vol. 111, no. 4, Jul. 2014, https://doi.org/10.14359/51686631.

[20] T. Wang and T. T. C. Hsu, "Nonlinear finite element analysis of concrete structures using new constitutive models," *Computers & Structures*, vol. 79, no. 32, pp. 2781–2791, Dec. 2001, https://doi.org/10.1016/S0045-7949(01)00157-2.

[21] Y. T. Obaidat, *Structural retrofitting of concrete beams using FRP*: debonding issues. Lund, Sweden: Lund University, 2011.

[22] Guide for the Design and Construction of Structural Concrete Reinforced with Fiber-Reinforced Polymer (FRP) Bars, ACI 440.1R-15, American Concrete Institute, Farmington Hills, MI, Mar. 2015.

[23] H. M. Salman and M. H. Al-Sherrawi, "Interaction Diagram for A Reinforced Concrete Column Strengthened with Steel Jacket," *International Journal of Civil Engineering and Technology*, vol. 10, no. 6, pp. 1369–1377, Jun. 2024.

[24] H. A. Hasan, M. N. Sheikh, and M. N. S. Hadi, "Maximum axial load carrying capacity of Fibre Reinforced-Polymer (FRP) bar reinforced concrete columns under axial compression," *Structures*, vol. 19, pp. 227–233, Jun. 2019, https://doi.org/10.1016/j.istruc.2018.12.012.

[25] M. N. S. Hadi, H. Karim, and M. N. Sheikh, "Experimental Investigations on Circular Concrete Columns Reinforced with GFRP Bars and Helices under Different Loading Conditions," *Journal of Composites for Construction*, vol. 20, no. 4, Aug. 2016, Art. no. 04016009, https://doi.org/10.1061/(ASCE)CC.1943-5614.0000670.

[26] A. Hadhood, H. M. Mohamed, F. Ghrib, and B. Benmokrane, "Efficiency of glass-fiber reinforced-polymer (GFRP) discrete hoops and bars in concrete columns under combined axial and flexural loads," *Composites Part B: Engineering*, vol. 114, pp. 223–236, Apr. 2017, https://doi.org/10.1016/j.compositesb.2017.01.063.

[27] S. Pessiki and A. Pieroni, "Axial Load Behavior of LargeScale Spirally Reinforced HighStrength Concrete Columns," *ACI Structural Journal*, vol. 94, no. 3, pp. 304–314, 1997, https://doi.org/10.14359/482.

[28] F. Abed, A. El-Refai, and N. El-Mesalami, "Compressive Behaviour of Glass Fiber-Reinforced Polymer (GFRP) Reinforced Concrete Columns," in *10th International Conference on FRP Composites in Civil Engineering*, Sharjah, UAE, 2022, vol. 198, pp. 851–858, https://doi.org/10.1007/978-3-030-88166-5_73.

[29] M. Elchalakani and G. Ma, "Tests of glass fibre reinforced polymer rectangular concrete columns subjected to concentric and eccentric axial loading," *Engineering Structures*, vol. 151, pp. 93–104, Nov. 2017, https://doi.org/10.1016/j.engstruct.2017.08.023.

[30] M. N. S. Hadi, H. A. Hasan, and M. N. Sheikh, "Experimental Investigation of Circular High-Strength Concrete Columns Reinforced with Glass Fiber-Reinforced Polymer Bars and Helices under Different Loading Conditions," *Journal of Composites for Construction*, vol. 21, Aug. 2017, Art. no. 04017005, https://doi.org/10.1061/(ASCE)CC.1943-5614.0000784.

[31] W. Abdelazim, H. M. Mohamed, and B. Benmokrane, "Inelastic second-order analysis for slender GFRP-reinforced concrete columns: Experimental investigations and theoretical study," *Journal of Composites for Construction*, vol. 24, no. 3, Art. no. 04020016, Apr. 2020.

[32] S. R. Razvi and M. Saatcioglu, "Strength and Deformability of Confined High-Strength Concrete Columns," *ACI Structural Journal*, vol. 91, no. 6, pp. 678–687, 1994, https://doi.org/10.14359/1499.